Neutron capture in ^{148,150}Sm: A sensitive probe of the *s*-process neutron density

K. Wisshak,* K. Guber, F. Voss, and F. Käppeler
Kernforschungszentrum Karlsruhe, Institut für Kernphysik, D-76021 Karlsruhe, Germany

G. Reffo
Comitato Nazionale dell'Energia Nucleare e dell'Energie Alternative, I-40138, Bologna, Italy
(Received 22 February 1993)

The neutron capture cross sections of ^{147,148,149,150,152}Sm were measured in the energy range from 3 to 225 keV at the Karlsruhe Van de Graaff accelerator using gold as a standard. Neutrons were produced via the ^{7}Li$(p,n)^{7}$Be reaction by bombarding metallic Li targets with a pulsed proton beam. Capture events were registered with the Karlsruhe 4π barium fluoride detector. Several runs were performed under different experimental conditions to study the systematic uncertainties in detail. For the first time, data were recorded with an ADC system that allows one to register gamma-ray energy and time of flight of the individual detector modules. The cross-section ratios were determined with an overall uncertainty of $\sim$1%. This is an improvement by about a factor of 5 compared to the existing data. Severe discrepancies were found with the results of previous measurements. Maxwellian-averaged neutron capture cross sections were calculated for thermal energies between $kT=10$ and 100 keV by normalizing the cross-section shape up to 700 keV neutron energy reported in literature to the present data. These stellar cross sections were used in an *s*-process analysis. The ratio of the values of the *s*-process current $\langle\sigma\rangle N_s$ (Maxwellian-averaged neutron capture cross section times *s*-process abundance) for the *s*-only isotopes ^{148,150}Sm is 0.870±0.009 rather than unity as expected by the local approximation. The corresponding branching in the *s*-process path is analyzed in the framework of the classical approach. The resulting mean neutron density, $n_n=(3.8\pm0.6)\times10^{8}$ cm^{-3}, is the most stringent value obtained so far. Finally the new cross sections are used to derive constraints for a stellar model and to check recently discovered isotopic anomalies in meteoritic samarium.

PACS number(s): 25.40.Lw, 28.20.Fc, 97.10.Cv

I. INTRODUCTION

The simultaneous availability of an improved setup for the accurate determination of neutron capture cross sections [1,2] and refined stellar model descriptions [3,4] makes studies of the synthesis of heavy elements in the so-called *s* (slow neutron capture) process a promising tool for the diagnostics of the stellar plasma of Red Giant stars. The analysis and interpretation of the isotopic pattern of the observed solar system abundances may yield the physical conditions during the *s* process, that is, temperature, neutron density, and matter density [5].

A first experiment on tellurium isotopes [6] confirmed the old prediction for the *s* process by Clayton *et al.* [7] of a "local approximation" (that the product of neutron capture cross section $\langle\sigma\rangle$ and *s*-process abundance N_s is constant for neighboring isotopes) with an uncertainty of $\sim$1%. This result strongly supports the idea of interpreting the (mostly small) deviations from this behavior as branchings in the neutron capture path of the *s* process. It is the analysis of such branchings that yields information on the physical conditions during the *s* process [5,6].

A prominent example is the branching in the samarium region that is illustrated in Fig. 1. Neutron capture in the unstable isotopes ^{147}Nd and ^{147,148,149}Pm causes a small part of the *s*-process flow to bypass ^{148}Sm. This implies that the ratio $N_s\langle\sigma\rangle(^{148}\mathrm{Sm})/N_s\langle\sigma\rangle(^{150}\mathrm{Sm})$ is slightly lower than unity, an effect that is determined mainly by the neutron density. It is obvious that a small deviation from unity can be determined reliably only if the respective cross sections $\langle\sigma\rangle$ and abundances N_s of ^{148}Sm and ^{150}Sm are known with sufficient accuracy. As can be seen from Fig. 1, ^{148}Sm and ^{150}Sm are *s*-only isotopes since they are shielded from contributions of the *r* process by their stable neodymium isobars. Thus the abundance ratio $N_s(^{148}\mathrm{Sm})/N_s(^{150}\mathrm{Sm})$ is identical to the

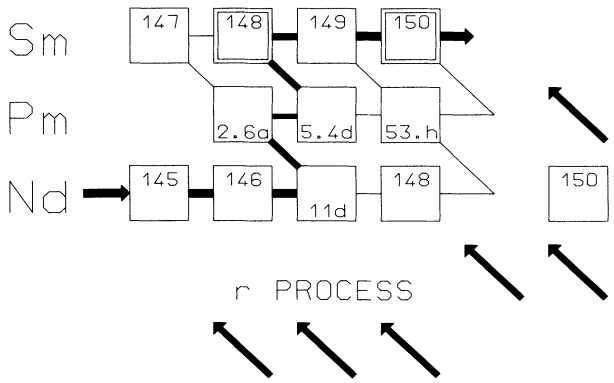

FIG. 1. The *s*-process path in the region of the samarium isotopes. The *s*-only isotopes ^{148,150}Sm are shielded from the *r* process by the stable isobars ^{148}Nd and ^{150}Nd. The unstable nuclei ^{147}Nd and ^{147,148,149}Pm are possible branching points.

*Author to whom correspondence should be addressed: Kernforschungszentrum Karlsruhe, Institut für Kernphysik III, Postfach 3640, D-76021 Karlsruhe, Germany.

isotopic ratio that is known to a precision of 0.1% [8]. Consequently, it is the uncertainty in the cross-section ratio, $\langle\sigma\rangle(^{148}\mathrm{Sm})/\langle\sigma\rangle(^{150}\mathrm{Sm})$, that determines the accuracy by which the *s*-process flow and, hence, the neutron density can be determined.

A detailed discussion of this branching was given by Winters *et al.* in 1986 [9]. In their work, the cross-section ratio was determined with an uncertainty of $\sim$4% resulting in an estimated strength for the neutron density of $(3.0\pm1.2)\times10^8$ cm^{-3}. The new experimental setup established at the Karlsruhe 3.75 MV Van de Graaff accelerator allows one to determine this ratio with an uncertainty of $\sim$1%, and thus to derive a more stringent value of the neutron density.

In addition, the absolute samarium cross sections are of general interest. Recently, it became obvious [10] that neutron capture cross-section measurements in the rare earth region were severely affected by the absorption of water in the oxide samples used in most experiments. This leads to a systematic overestimation of the cross section, and could explain why previous results vary by up to factors of 2 [11]. This finding calls for new measurements with very well characterized samples. Measurements on the odd samarium isotopes are further complicated by the fact that these nuclei exhibit a high binding energy ($\sim$9 MeV) and a very high average mutliplicity of the capture cascades ($\sim$5). Thus the capture gamma-ray spectra are soft. This may lead to systematic uncertainties in experiments using the pulse height weighting technique and a gold standard (see Sec. IV).

The aim of the present investigations was to derive improved neutron capture cross sections of the *s*-only samarium isotopes ^{148}Sm and ^{150}Sm. These data, together with the respective results on tellurium and barium isotopes that are already available [6] or presently under evaluation, will allow one to define the $\langle\sigma\rangle N_s$ curve in the region of the magic neutron shell, $N=82$. Secondly, the accurate determination of the cross-section ratio will allow a reanalysis of the branchings at $A=147-149$ in the framework of the classical *s*-process approach and with a stellar model to derive new constraints for the *s*-process neutron density.

In the following we describe the experiment, the sample preparation, and data evaluation in Secs. II and III. The differential cross sections are presented in Sec. IV, while the uncertainties are discussed in Sec. V. Section VI is devoted to the determination of stellar cross sections, and the implications for the classical *s*-process approach are given in Sec. VII. A further discussion of the consequences for current stellar models will be the topic of a forthcoming publication. A fully detailed description of the present experiment, data evaluation, calculation of correction factors, and the results of individual runs and evaluation methods can be found in Ref. [12].

II. EXPERIMENT

A. Experimental method

The neutron capture cross sections of the samarium isotopes 147 to 150 and 152 were measured in the energy range from 3 to 225 keV using gold as a standard. The experimental method has been published in detail in Refs. [1] and [2]. Here, only the most essential features are repeated and changes or improvements that were introduced since our measurement on the tellurium isotopes [6] are described. Neutrons were produced via the ^{7}Li$(p,n)^7$Be reaction by bombarding metallic Li targets with the pulsed proton beam of the Karlsruhe 3.75 MV Van de Graaff accelerator. The neutron energy is determined by time of flight (TOF), the samples being located at a flight path of 78 cm. The important parameters of the accelerator are pulse width $\sim$1 ns, repetition rate 250 kHz, and average beam current 1.5–2 μA. In different runs, the energy of the proton beam was adjusted to 30 and 100 keV above the reaction threshold of the ^{7}Li$(p,n)^7$Be reaction at 1.881 MeV. This yields continuous neutron spectra in the energy range of interest for *s*-process studies, i.e., 3–100 keV, and 3–200 keV, respectively. The use of different spectra allows one to optimize the signal to background ratio in different neutron energy regions (see Sec. III).

The Karlsruhe 4π barium fluoride detector was used for the registration of capture gamma-ray cascades. This detector (a comprehensive description is given in Ref. [1]) consists of 42 hexagonal and pentagonal crystals forming a spherical shell of BaF_2 with 10 cm inner radius and 15 cm thickness. It is characterized by a resolution in gamma-ray energy of 7% at 2.5 MeV, a time resolution of 500 ps, and a peak efficiency of 90% at 1 MeV. Capture events are registered with $\sim$95% probability.

In one run of the present experiment, a newly implemented ADC system was used for data acquisition [13]. This system is based on CAMAC modules of type FERA (Le Croy). It allows the storage of the gamma-ray energy and TOF information of the individual detector modules that have fired in a particular event. A special preprocessing procedure rejects events in selectable sum energy and TOF regions; this decision is made within 4 μs. The hardware trigger is made by a combination of ALU (arithmetic logic unit) and MLU (multiplicity logic unit) modules. Accepted events are transmitted from a data stack to a set of two memories that are mutually used for input and output. The ADC system in conjunction with the preprocessing is able to accept count rates up to 60 kHz. The recorded events are transmitted from the experiment computer (Data General MV 4000) to a work station (Silicon Graphics IRIS) via ethernet file transfer. There the events are stored either on optical disc or on DAT tape for further evaluation.

The purpose of the ADC system is fourfold. (i) It allows us to measure capture cascades and capture gamma-ray spectra directly. This information is necessary to determine the detector efficiency for capture events and had to be taken from theoretical calculations previously [2]. (ii) It allows a deeper understanding of the capture process, e.g., by determining angular or multiplicity distributions of capture gamma rays. (iii) It reduces significantly the recorded event rate by rejecting events in sum energy and TOF regions that are not needed for the evaluation of the cross section (see Sec. III). (iv) It allows us to improve the resolution in gamma-ray sum energy by

off-line corrections of the nonlinearity of individual detector modules.

The main advantages of using a 4π BaF_2 detector in combination with a Van de Graaff accelerator are the following: The entire capture cascade is detected with good energy resolution. Thus, ambiguities in the detection efficiency due to different cascade multiplicities are avoided, and neutron capture events can be separated from gamma-ray background, and from background due to capture of sample scattered neutrons, by selecting events with appropriate sum energy. The high granularity of the detector allows a further separation of capture events and background by means of the recorded event multiplicity. The short primary flight path and the inner radius of the detector guarantee that part of the TOF spectrum is completely undisturbed by background from sample-scattered neutrons (see Sec. III). This range with optimum signal to background ratio can be used to normalize the cross section. The high detection efficiency allows the use of small samples, avoiding large multiple scattering corrections. Finally, the ^{7}Li(p,n) reaction yields neutrons exactly and exclusively in the range of interest for *s*-process studies.

B. Samples

Isotopically enriched samples were prepared from Sm_2O_3 powder. The relevant parameters of the eight samples are compiled in Table I. In addition to the five samarium samples a gold sample, a graphite sample, and an empty position in the sample changer frame were used in all runs. In one run, the small gold sample (Au I) and, in the two others, the larger sample (Au II) were used. The respective sample masses were selected according to the expected cross sections in order to obtain similar capture yields in all cases. The sample masses could be reduced by factors of 3 to 4 compared to those used by Winters *et al.* [9]. Hence, sample-related uncertainties, i.e., for multiple scattering and self-shielding corrections, are significantly smaller. The isotopes ^{147}Sm, ^{149}Sm, and ^{152}Sm were included in the measurements to correct the data for the *s*-only isotopes ^{148}Sm and ^{150}Sm for isotopic impurities.

The exact characterization of the sample is a severe problem for accurate cross section measurements [14]. This was particularly difficult in the present case since samarium oxide is hygroscopic. The absorption of water in the samples can produce a serious deterioration in capture cross-section measurements [10]. Therefore, the pellets pressed from oxide powder were heated to 1000 deg under a steady flow of dry air, and their weight determined immediately afterwards. Then, the pellets were kept in a dry atmosphere until they were welded into thin polyethylene foils to avoid further absorption of water. During the heating, there was a significant loss in weight (4–14 %). After a slight increase during the first days of $\sim$0.2%, the samples were very stable over the measuring period of $\sim$6 months. The observed increase in weight was assumed to be due to absorption of water at the surface of the samples. The respective contamination is given in the fifth column of Table I.

After the experiment, the material was carefully analyzed to confirm the low contamination with water and to look for possible deviations from the assumed stoichiometry. The exact samarium concentration was determined by means of the method of *K*-edge densitometry [15,16]. A well collimated beam of x rays with a continuous energy distribution passes through the liquid sample in a well defined geometry. The x-ray spectrum is observed with a HPGe detector and the concentration is determined from the step at the *K* edge. For calibration two types of standard solutions were prepared, covering the concentration range of the actual solutions. One set was prepared from natural Sm_2O_3 by producing pellets in exactly the same way as for the enriched samples. The other set was prepared from samarium metal that was handled in a glove box filled with argon. The concentration was calculated under the assumption that the dissolved material is pure Sm_2O_3 or Sm, respectively. The uncertainties of the individual measurements are 0.4%, mainly determined by filling the 10 ml volumetric flasks used for preparation of the solutions. From the results,

TABLE I. Compilation of relevant sample data.

Sample[a]	Thickness (mm)	Thickness[b] (10^{-3} atoms/b)	Weight (g)	Water[c] content (%)[f]	Canning[d] (mg)	Impurity[e] (%)[f]	Neutron binding energy (MeV)
Au I	0.26	1.5067	0.8708		5.4		6.513
Au II	0.4	2.2474	1.2989		7.2		
Graphite	4.0	34.320	1.2096				
^{147}Sm	0.6	0.9255	0.3993	0.23	7.2	<0.2	8.141
^{148}Sm	2.6	4.5331	1.9694	0.17	8.9	<0.2	5.872
^{149}Sm	1.0	1.7294	0.7563	0.14	7.3	<0.2	7.986
^{150}Sm	2.2	3.0603	1.3474	0.22	8.1	<0.2	5.597
^{152}Sm	1.9	3.2253	1.4387	0.14	8.0	<0.2	5.867

[a]Samples of 15 mm diameter.
[b]For samarium samples: sum of all Sm isotopes (oxygen not included), chemical composition Sm_2O_3.
[c]As determined from the increase in weight of the samples.
[d]Polyethylene foil (CH_2).
[e]Impurity of other elements except oxygen.
[f]% of weight.

the following conclusions can be drawn: The average of the four measurements with standard sources prepared from samarium metal or samarium oxide agree within 0.17%. This is strong evidence that the oxide samples contain no water or other impurities at the time immediately after heating, when the weight was determined; the same holds for the enriched samples, as well. The results for the enriched samples are compatible with the calculated concentration within their uncertainty of 0.4%. The only exception is the result for ^{147}Sm where the measured concentration is too high by about 1%. This could be explained only if the specified stoichiometry of the material was incorrect, e.g., by a samarium excess in the sample.

A second batch of the sample material was analyzed in the analytic laboratory of the Material Research Department at KfK for its water content. According to the coulometric method of Fischer, the water was extracted from the samples at 900 deg in a stream of nitrogen gas and collected in a coulometric measuring cell. The amount of water was then determined by titration. The samarium content was determined for a second time by x-ray fluorescence analysis using the method of borax discs. The respective results are completely independent of the x-ray absorption experiment and slightly more accurate. The measurement was calibrated by preparing standard discs from high purity natural samarium in exactly the same way as for the enriched isotopes. Within the quoted uncertainties of 0.2–0.3 %, the results of the water and samarium determination add up to 100%. The amount of water found in the samples is in good agreement with the contamination determined from the increase in sample weight given in Table I. No deviation in stoichiometry of the ^{147}Sm sample was observed in this analysis.

There is still one drawback that has to be discussed in more detail. Packing of the samples in thin polyethylene foils helped to prevent further absorption of water during the experiment, but is certainly not ideal as it adds hydrogen to the samples. The polyethylene weights are given in Table I, and seem to be significant compared to the total sample masses. However, one has to keep in mind that neutron scattering in hydrogen goes mainly in the forward direction with a maximum scattering angle of 90°. Thus, only neutrons scattered in the upstream part of the packing will hit the sample. The weight of this part is 1.8 mg corresponding to 2.3 mg water. This is about 0.2% of the sample mass, and is thus of the same size as the water content of the samples given in Table I. The contribution of the packing to the uncertainty of the measured data will be discussed in Sec. V.

As a third step in characterizing the samples, the isotopic composition was redetermined at KfK. The results are compiled in Table II. The agreement with the data provided by the suppliers is within 0.1%.

The diameter of the samples was 15 mm. As can be seen from Table I, the thickness of some samples is comparatively large, and the transmission decreases down to 0.90. Since accurate data for the total cross section of the samarium isotopes were not available from literature, the spectra measured with the neutron monitor at 260 cm flight path did not allow a check of the normalization of the neutron flux as in our first measurement [2]. However, since the scintillator of this neutron monitor is completely shaded by the sample, the measured TOF spectra can in turn be used for a rough determination of the total cross section. Though the accuracy of this method is inferior to that obtained in a dedicated experiment, the data are sufficient for the reliable calculation of the multiple scattering corrections (see Sec. III).

C. Measurements

The samples were moved cyclically into the measuring position by a computer-controlled sample changer. The data acquisition time per sample was about 10 min, a complete cycle lasting about 1.5 h. From each event, a 64-bit word was recorded on magnetic tape containing the sum energy and TOF information, together with 42 bits indicating those detector modules that have contributed. As mentioned above, two runs have been performed using neutron spectra with different maximum energy. For the first time, the data in run III were recorded with an ADC system. In this case gamma-ray energy and TOF were stored for all detector modules. An automatic offset suppression guaranteed that only those modules that contributed significantly to an event were read out. The maximum neutron energy was chosen at 200 keV as in run II. In this way, the two methods could be checked against one another under identical experimental conditions. In runs I and II, 120 high density tapes of data containing roughly 20 Gbyte of information were recorded; in run III, where the information to be stored per event is much larger, the total amount of data was 8 Gbyte. The increased amount of information stored per event is compensated by the preprocessing that rejects about 50% of the events. The spectra of the two neutron monitor detectors were stored on magnetic disk.

TABLE II. Isotopic enrichment of the samarium samples (%).

	Isotope						
Sample	144	147	148	149	150	152	154
^{147}Sm	0.05	98.27	0.85	0.36	0.11	0.22	0.14
^{148}Sm	0.08	1.00	95.31	2.61	0.37	0.42	0.21
^{149}Sm	0.05	0.22	0.82	96.70	1.51	0.48	0.22
^{150}Sm	0.06	0.41	0.46	1.14	94.87	2.38	0.68
^{152}Sm	0.02	0.10	0.15	0.12	0.15	98.88	0.58

III. DATA EVALUATION

A. Total cross sections

The total cross sections of the samarium isotopes were determined in the neutron energy range from 10 to 200 keV from the TOF spectra measured with the lithium glass neutron monitor at a flight path of 260 cm. The difference of the count rates recorded with and without sample are small, but statistics are excellent due to the large acquisition time of the capture measurement. The count rate in each TOF channel t is composed of three parts ${}^xC(t)={}^xC1(t)+{}^xC2(t)+{}^xC3$, where index x labels the samples, $x=0$ being the empty position. $C1$ is the measured effect due to primary neutrons reacting in the lithium glass, while $C2$ is a time-dependent background caused by neutrons scattered from the detector material into the scintillator. $C3$ is a time-independent background due to moderated neutrons. The transmission T and the total cross section σ of sample x with thickness n is simply given by

$$ {}^xT=e^{-n(x)\sigma(x)}={}^xC1/{}^0C1 \ . $$

While the time-independent background can easily be determined from the count rate at very large TOF, certain assumptions had to be made for the time-dependent background $C2$. We assumed that $C2$ at energy E is proportional to the integral number of neutrons hitting the sample in the energy interval from E to $E_{\max}$, and that this flux is proportional to the average transmission $\langle T(E \text{ to } E_{\max})\rangle$ in this energy interval. If, as for the present samples, the transmission is very high, it is in lowest approximation energy independent. To this approximation, the background $C2$ is proportional to $T(E)$, as is the count rate $C1$, and can, therefore, be neglected. In other words, with the assumptions made above, the transmission is independent of $C2$. The approximation $\langle {}^xT(E \text{ to } E_{\max})\rangle = {}^xT(E)$ is thus justified since the background is much smaller than the measured effect ($C1 \gg C2$).

The resulting total cross sections of all samples are given in Table III. They were calculated using the total cross section for oxygen from the JEF (joint evaluated file) evaluation [17]. The results for the carbon sample are systematically lower by 3% compared with the data from JEF. This deviation was adopted as a reasonable systematic uncertainty of the present experiment for a sample with 86% transmission. In all other samples the absorption $A=1-T$ is much smaller, and consequently higher systematic uncertainties are quoted in Table III, assuming a $1/A$ dependence. Compared to that effect, statistical uncertainties can be neglected. The total cross section of elemental samarium calculated from our isotopic cross sections is in reasonable agreement with the data of Ref. [18]. The gold cross section is systematically larger, as given in Ref. [18], but in the energy range from 10 to 100 keV the available data were from an experiment made in 1965 [19]. The total cross sections are important for the proper correction of neutron multiple scattering effects in the capture experiment (see below).

B. Evaluation of the capture cross sections

The data evaluation has been described in detail in Ref. [2]. All events stored on magnetic tape were sorted into two-dimensional sum energy versus TOF spectra according to event multiplicities (evaluation 1). In evaluation 2, this procedure was repeated by rejecting those events, where only neighboring detector modules contributed to the sum energy signal, in order to reduce background from the natural radioactivity of the BaF_2 crystals and from capture of scattered neutrons in the BaF_2 scintillator material. These spectra were normalized to equal neutron flux using the count rate from the lithium glass monitor, which was located close to the neutron target; these normalization factors are in general well below 1%.

The calculation of the two-dimensional spectra from the data recorded with the ADC system is slightly more complicated. The energy and TOF scales of the 42 detector modules were calibrated before and after the experiment. In addition, we used sources of ^{228}Th, Am+Be, and Pu+^{13}C to determine possible deviations of the energy calibration from linearity for each detector module. During the sorting procedure, events were accepted only if energy and TOF information were recorded from the contributing detector modules. The gamma-ray energies of the individual modules were corrected for their respective nonlinearities. Then, the measured offset was sub-

TABLE III. The total cross sections determined from the count rate of the ^{6}Li glass neutron monitor at 260 cm flight path.

Neutron energy (keV)	Total cross section (b)						
	^{147}Sm	^{148}Sm	^{149}Sm	^{150}Sm	^{152}Sm	C	^{197}Au
10–15	36.0	19.4	25.5	24.8	15.2	4.39	18.9
15–20	25.9	17.6	22.1	21.7	12.8	4.40	16.6
20–30	25.4	16.6	19.9	18.0	14.9	4.51	17.1
30–40	23.6	15.5	17.9	16.1	11.7	4.36	14.9
40–60	20.4	12.9	16.1	15.5	11.8	4.48	14.7
60–80	17.0	12.8	13.3	13.9	10.5	4.35	13.1
80–100	14.8	12.8	13.4	11.7	9.7	4.13	12.4
100–150	15.0	10.3	11.6	11.7	9.5	4.17	11.5
150–200	11.8	9.3	10.1	11.2	8.9	4.10	10.5
Uncertainty	18%	5%	11%	6%	7%	3%	13%

tracted and the gain was transformed to the average value of all modules. Finally, the sum energy of the event could be calculated by adding the individual gamma-ray energies of the cascade. The TOF information of all modules was similarly transformed to a mean time calibration and a common position of the prompt gamma-ray peak that indicates the zero point of the time measurement. The shortest TOF value of all contributing modules was taken as representative for the event. Thus gamma rays scattered from one detector module into another do not cause a deterioration of the time resolution.

In the next step, the spectra measured without sample were subtracted to remove the sample-independent background. The remaining time-independent background was determined at very long flight times (~ 3.9 μs), where no time-correlated events are expected. Two-dimensional spectra of run III containing all events with multiplicity >2 are shown in Fig. 2. Note, that in the spectra the events at low sum energy and large TOF are suppressed by the hardware trigger of the ADC system.

At this point, the spectra contain only events that are correlated with the sample. The next correction to be made was for isotopic impurities. In contrast to neutron capture experiments without resolution in gamma-ray energy [9], the contribution to isotopic impurities has to be eliminated from the measured spectra before evaluating the correction for scattered neutrons or determining the capture yield. This is important because the respective events are located predominantly at different sum energies. Therefore, the spectra of the impurity isotopes were subtracted after normalizing them to their respective abundance in the sample under investigation. These coefficients are compiled in Table IV. The isotopes ^{144}Sm and ^{154}Sm were not included in the present experiment. The effect of ^{144}Sm was neglected in the analysis since the respective impurities are less than 0.1% in all samples (see Table II), and since the cross section is at least a factor of 3 smaller than for all other isotopes [11]. The correction for ^{154}Sm was treated as for ^{148}Sm, since this isotope has about the same binding energy, but the abundance was scaled by a factor of 1.1 to account for the slightly larger cross section. The impurity of this isotope is always smaller than 1%; therefore, this assumption does not affect the results. The coefficients in the correction matrix are in general of the order of 1% or less. The worst case is ^{148}Sm, where—according to Table IV—the corrected spectrum is calculated by

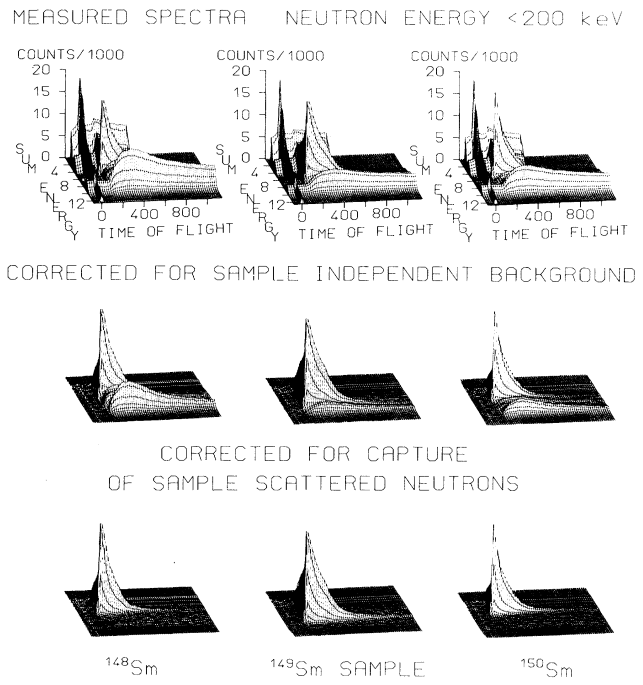

FIG. 2. The different steps of background subtraction in the two-dimensional sum energy times the TOF spectra. The data are shown for three samarium isotopes measured in run III with 200 keV maximum neutron energy. (The original resolution of 128×2048 channels was compressed in the plots into 64×64 channels.) Note that events with low sum energy and large TOF are suppressed by the preprocessing of the data.

$$^{148}\mathrm{Sm}_{\mathrm{corr}} = {}^{148}\mathrm{Sm}_{\mathrm{meas}} - 0.049\times{}^{147}\mathrm{Sm}_{\mathrm{meas}} - 0.070\times{}^{149}\mathrm{Sm}_{\mathrm{meas}} - 0.004\times{}^{150}\mathrm{Sm}_{\mathrm{meas}} - 0.005\times{}^{152}\mathrm{Sm}_{\mathrm{meas}} \ .$$

The capture yields of the samples are about equal except for the ^{149}Sm sample where it is a factor of 2 larger. At first glance, the above equation seems to imply that the ^{148}Sm yield is reduced by $\sim 20\%$. Actually, the reduction is $<8\%$ as most of the count rate in the ^{149}Sm and ^{147}Sm spectra is located near the binding energy of 8 MeV, a region that is not used for the evaluation of the ^{148}Sm cross section (binding energy 5.8 MeV). It has to be mentioned that in an experiment using the pulse height weighting technique, where no energy information is available [9], and where the efficiency is proportional to the binding energy, the corresponding correction would be about 30% of the observed effect, a factor of 4 larger than in the present case. The isotopic correction for the ^{148}Sm sample, which is the worst case, is shown in Fig. 3. There, the TOF spectrum used for the determination of the cross section shape (see below) is plotted together with the count rate that is removed by the isotopic correction.

In the corrected spectrum, e.g., of ^{148}Sm, which was calculated using the matrix elements in Table IV, not only the isotopic impurities are eliminated, but also the effect of the main isotope is reduced. This is because the spectra measured with the other samples contain ^{148}Sm as an impurity. In the final analysis, this effect was included by a corrected sample thickness, given in the last column of Table IV.

After the correction for isotopic impurities, the background due to capture of sample scattered neutrons was removed from the spectra by means of the data measured with the carbon sample. The scattered neutrons are captured mainly in the odd barium isotopes of the scintillator (binding energy ~ 9 MeV). The binding energy of the

TABLE IV. Matrix for the isotopic correction (%).[a]

Corrected spectrum	Measured spectrum ^{147}Sm	^{148}Sm	^{149}Sm	^{150}Sm	^{152}Sm	Corrected sample thickness (10^{-3} atom/b)
^{147}Sm	100	−0.2107	−0.1832	−0.0324	−0.0586	0.9095
^{148}Sm	−4.9493	100	−7.0138	−0.4068	−0.5407	4.3326
^{149}Sm	−0.3486	−0.3977	100	−0.8305	−0.1959	1.6750
^{150}Sm	−1.2870	−0.8746	−1.9396	100	−2.1944	2.9066
^{152}Sm	−0.3260	−0.5180	−0.1908	−0.1512	100	3.1929

[a]Using the approximation $\sigma(^{144}\text{Sm})=0$ and $\sigma(^{154}\text{Sm})=1.10\sigma(^{148}\text{Sm})$

even samarium isotopes, being below 5.9 MeV, allows an efficient background reduction to be made because neutron captures in the barium isotopes are well separated by their sum energy from the true capture events in the sample. Actually, the sum energy range from 6.6 to 9.6 MeV could be used for normalizing the scattering correction. This normalization is calculated as a function of the TOF, which is very important for the accuracy of the experimental method. After this correction, the spectra contain true capture events only (lower part of Fig. 2), and can be used to determine the cross sections. The binding energies of the odd samarium isotopes are 8.1 and 7.9 MeV, respectively; thus the lower end of the normalization interval had to be increased to 8.9 MeV. This comparatively small interval was still sufficient for determination of reliable corrections.

The corrections for sample scattered neutrons are illustrated in Fig. 4. The TOF spectra of the ^{148,149,150}Sm samples are plotted after projection of the two-dimensional data in the sum energy range around the binding energy (see below) together with the background

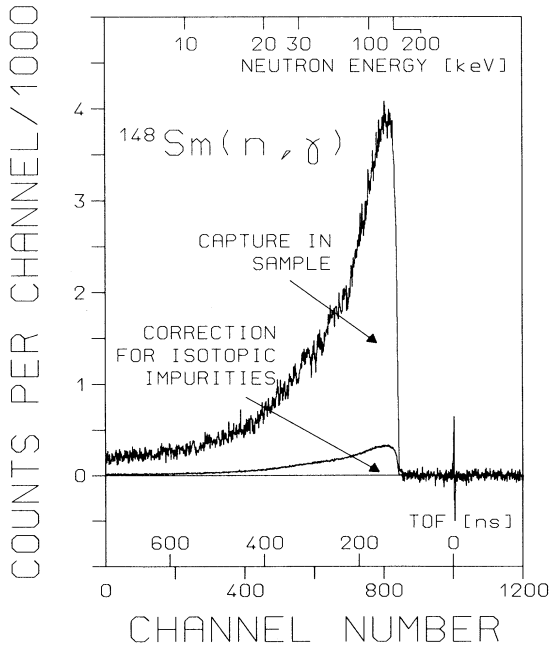

FIG. 3. TOF spectrum measured with the ^{148}Sm sample. The background due to isotopic impurities is shown separately.

due to capture of sample scattered neutrons. The data are given for run I with 100 keV maximum neutron energy. The large cross sections of the samarium isotopes allowed the cross section to be evaluated down to 3 keV.

After subtraction of the background, the TOF spectra shown in Fig. 4 were used to determine the shape of the cross section. For normalization, the two-dimensional spectra were projected on the sum energy axis in the region of optimum signal to background ratio as indicated by dashed boxes in Fig. 4. The result is shown in Fig. 5 where the events with multiplicity >2 are plotted for all isotopes.

In Fig. 6, the sum energy spectra of ^{148}Sm and ^{149}Sm are shown as a function of the detector multiplicity. A multiplicity ≥ 5 is observed for $\sim 40\%$ of the events in the even and for $>80\%$ in the odd samarium isotopes. Gamma-ray background mainly affects the spectra with multiplicity 1 and 2, giving rise to large statistical fluctuations below ~ 3 MeV (channel number 40). These figures demonstrate the potentials of the detector as a multiplicity filter, separating capture events with high multiplicity from gamma-ray background with low multiplicity. An extreme case is found for ^{149}Sm where the level density is so large that nearly all events are registered with multiplicity ≥ 5.

The arrows in Fig. 6 indicate the range of sum energy channels that were combined to yield the TOF spectra given in Fig. 4, which were then used to determine the cross-section shape. Thus the sum energy range below the lower arrow is not used in the evaluation, except in the TOF interval used for the absolute normalization (dashed box in Fig. 4). The preprocessing of the ADC system rejects the events at low sum energy and large TOF, which are not required for data analysis. In this way, the recorded event rate is reduced by approximately a factor of 2 (see Fig. 2).

The cross-section ratio of isotope X relative to the gold standard is then

$$\frac{\sigma_i(X)}{\sigma_i(\text{Au})}=\frac{Z_i(X)}{Z_i(\text{Au})}\frac{\sum Z(\text{Au})}{\sum Z(X)}\frac{\sum E(X)}{\sum E(\text{Au})}\frac{m(\text{Au})}{m(X)}F_1F_2\ . \tag{1}$$

In this relation, Z_i is the count rate in channel i of the TOF spectrum, $\sum Z$ is the integral TOF count rate in the interval used for normalization (see Fig. 4), $\sum E$ is the total count rate in the sum energy spectrum for all multipli-

cities summed over the normalization interval (see Fig. 6), and m is the sample thickness in atoms/b. The factor $F_1=[100-f(\mathrm{Au})]/[100-f(x)]$ corrects for the capture events f below the experimental threshold in the sum energy, where x refers to the respective samarium sample (Table V), and F_2 is the respective ratio of the multiple scattering and self-shielding corrections (Table IV).

The fraction of unobserved capture events f and the correction factor F_1 were calculated as described in detail in Ref. [2]. For this purpose, two kinds of information are necessary: (1) the individual neutron capture cascades and their relative contribution to the total capture cross section, and (2) the detector efficiency for monoenergetic gamma rays in the energy range up to 10 MeV.

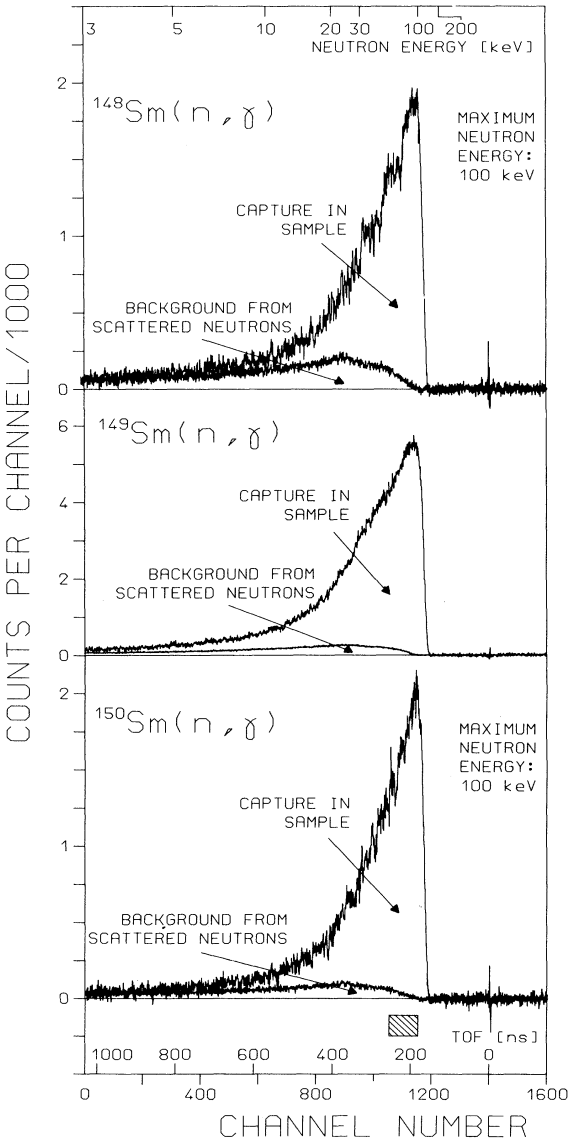

FIG. 4. TOF spectra measured with three samarium samples in run I with 100 keV maximum neutron energy. The background due to capture of sample scattered neutrons is shown separately. The region used for the absolute normalization of the cross sections are shown by the hatched box.

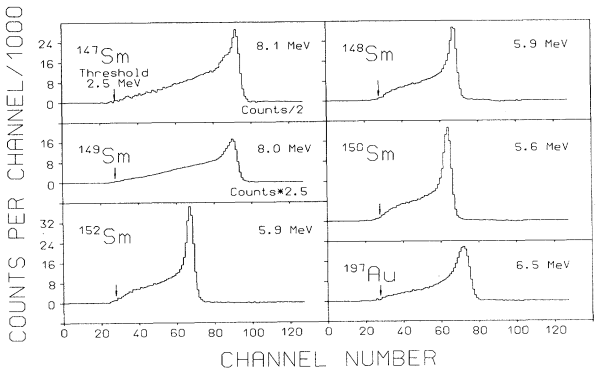

FIG. 5. Sum energy spectra of all isotopes measured in run II containing all events with multiplicity >2. These spectra were obtained by projection of the two-dimensional spectra in the TOF region below the maximum neutron energy as indicated by the hatched box in Fig. 4.

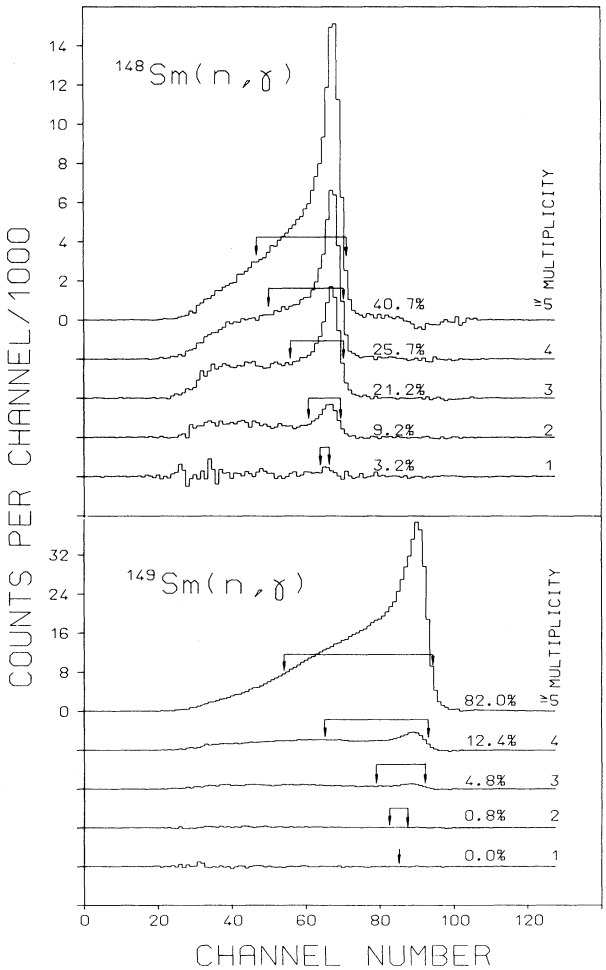

FIG. 6. Sum energy spectra from the ^{148}Sm and ^{149}Sm sample in dependence of detector multiplicity (the same data as shown in Fig. 5). The regions used to determine the cross-section shape are indicated by arrows.

Capture cascades and capture gamma-ray spectra of the involved isotopes were calculated according to the statistical and optical model [20]. In Ref. [12], the cross section is given as a function of the cascade multiplicity together with the gamma-ray energies of the 20 most probable cascades of the samarium isotopes. The corresponding data for gold have been given already in Ref. [2]. The first 20 cascades yield 16–23 % of the cross section, but up to 2400 are necessary to cover 95%. The average multiplicity of the cascades ranges from 3.8 to 5.0.

The efficiency of a BaF_2 shell for monoenergetic gamma rays was calculated in Ref. [21] with various assumptions for multiple Compton events, resulting in optimistic and pessimistic estimates for the peak efficiency, SW(MAX) and SW(MIN). The data given in Ref. [2] were used to calculate the fraction f of unobserved capture events (see Table V). The time to calculate the sum energy spectrum of a capture cascade scales with multiplicity m according to 20^m, since each gamma ray is divided into 20 energy bins [2]. Thus the computer time is completely dominated by the number of cascades with multiplicity 6 and 7. For the tellurium isotopes [6], only a few percent of the cross section is from cascades with multiplicity 6, but for ^{149}Sm about 10% of the cross section involves cascades with multiplicity 7. Thus the high multiplicity of the capture cascades, especially of the odd samarium isotopes, prohibited making these calculations on the central IBM 3090 M computer of our research center that was used in the previous work. Instead, we used a multitransputer system [22] of our department that contains 24 T800 transputers, each equipped with a working processor and 4 Mbyte RAM memory, sufficient to run rather large codes. The total computing power of this machine is comparable with that of the IBM 3090M but has the advantage of a single-user machine. Therefore, it was feasible to perform the full calculation for all samarium isotopes. The total computing time for ^{149}Sm was about 20 days. In addition, it was possible to repeat the calculations for the gold standard with all cascades, which has been too expensive in the past [2].

In the actual measurements, we used a threshold in the sum energy of 2.4 MeV in runs I and III, and of 2.5 MeV in run II. Accordingly, the efficiency of the detector was

TABLE V. Calculated fraction of unobserved capture events, f (%), and the corresponding correction factors, F_1, for the cross-section ratios.

Sample	Threshold in sum energy (MeV) 2.0	2.4	2.5	Assumption for gamma-ray efficiency
Solid angle 94%, gamma-ray threshold 50 keV				
f(Au)	4.99		7.25	SW(MAX)
f(^{147}Sm)	0.55		1.27	
f(^{148}Sm)	3.84		6.75	
f(^{149}Sm)	1.10		1.76	
f(^{150}Sm)	4.81		8.18	
f(^{152}Sm)	5.26		7.45	
f(Au)	5.78		8.35	SW(MIN)
f(^{147}Sm)	0.78		1.73	
f(^{148}Sm)	5.00		8.30	
f(^{149}Sm)	1.29		2.05	
f(^{150}Sm)	6.07		9.98	
f(^{152}Sm)	6.16		9.09	
f(Au)	5.28		7.61	From
f(^{147}Sm)	0.74		1.28	experiment
f(^{148}Sm)	4.67		7.25	(Ref. [23])
f(^{149}Sm)	0.87		1.54	
f(^{150}Sm)	5.34		8.45	
f(^{152}Sm)	5.00		7.46	
F_1(^{147}Sm/Au)	0.953	0.939	0.936	$\frac{1}{2}$SW(MAX)+
F_1(^{148}Sm/Au)	0.990	0.996	0.997	$\frac{1}{2}$SW(MIN)
F_1(^{149}Sm/Au)	0.958	0.944	0.940	
F_1(^{150}Sm/Au)	1.000	1.011	1.014	
F_1(^{152}Sm/Au)	1.010	1.006	1.005	
F_1(^{147}Sm/Au)	0.954	0.941	0.936	From
F_1(^{148}Sm/Au)	0.994	0.995	0.996	experiment
F_1(^{149}Sm/Au)	0.956	0.943	0.938	(Ref. [23])
F_1(^{150}Sm/Au)	1.001	1.007	1.009	
F_1(^{152}Sm/Au)	0.997	0.998	0.998	

98% for the odd and 92% for the even isotopes. It has to be noted that, for the present experimental method, it is not necessary to know the absolute efficiency of the detector, which depends on the efficiency for monoenergetic gamma rays. As can be seen from Table V, differences of about 2% are observed in the even isotopes for the different assumptions SW(MAX) and SW(MIN). Since sample and standard are measured with the same detector, the final correction factors F_1 are practically insensitive to the assumed detector efficiency. For the even isotopes, which have binding energies similar to the gold standard, the correction is very small; only for the odd isotopes are differences in efficiency of several percent found. In Fig. 7, the calculated sum energy spectra are shown separately for the two different assumptions of the detector efficiency. Comparison with Fig. 5 demonstrates that the experimental results are indeed between these two extremes.

While this work was submitted for publication, experimental information on the gamma-ray efficiency of the Karlsruhe 4π BaF_2 detector became available (Ref. [23]). The line shape of monoenergetic gamma rays was measured in the energy range from 0.8 to 8.4 MeV. The gamma rays were produced by (p,γ) reactions on thin ^{26}Mg, ^{30}Si, and ^{34}S targets. By selecting appropriate proton energies, resonances were excited, which decay predominantly by cascades of two gamma transitions. These cascades were observed in coincidence with a germanium detector resulting in two-dimensional spectra, $E_\gamma(\text{Ge}) \times E_\gamma(\text{BaF}_2)$. The response of the 4π BaF_2 detector for monoenergetic gamma rays was obtained by selecting those events, where the full energy of the complementary gamma quant is registered in the germanium detector.

Spectra were recorded from seven (p,γ) resonances and from a ^{88}Y source, yielding the line shape of 20 gamma transitions in the energy range from 0.843 to 8.392 MeV. With these data, the calculation of the spectrum fraction f and of the correction factor F_1 were repeated (Table V). Very good agreement is found between the results for F_1 calculated from experimental and theoretical values for the detector efficiency (see Table V). In the final evaluation of the cross sections we used the results obtained with the experimental detector efficiency.

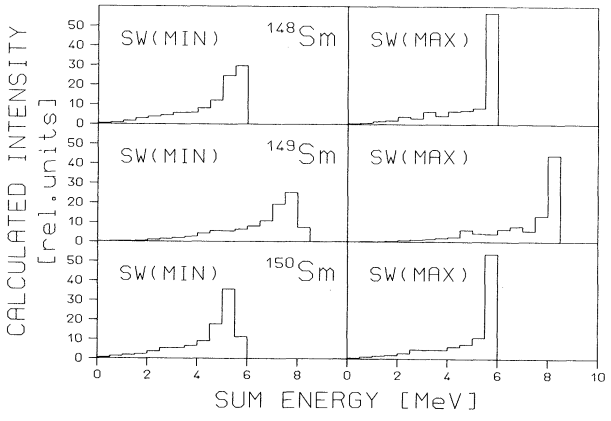

FIG. 7. Calculated sum energy spectra of the 4π BaF_2 detector as obtained under different assumptions on the detector efficiency. These spectra were used to derive the correction F_1 for unobserved capture events.

During this work it became obvious that in unfavorable cases the result for the spectrum fraction may significantly depend on the random numbers that were used to simulate the finite solid angle of 94% of the detector. Therefore all calculations for the gold sample and the even samarium isotopes were repeated using three sets of random numbers produced by three different generators. The data given in Table V are the average of the three calculations. These values, therefore, are slightly different from the preliminary data given in Ref. [12].

The correction for multiple scattering and self-shielding in the sample was calculated with the SESH code [24]. The input data for the pairing energies were taken from Ref. [25]. The main problem is to find parameter sets that reproduce not only the capture cross section, but the total cross section of each isotope as well. We started from the parameters given by Mughabghab [26]. These data were changed so that the total cross sections of Table III were reproduced within an uncertainty of $\sim 3\%$, and our data for the capture cross sections within $\sim 10\%$. The respective input parameters, the results for the total cross sections, and the values for the multiple scattering correction are compiled in Ref. [12]. In all calculations, oxygen was included by assuming the stoichiometry to be Sm_2O_3. The correction factors F_2 are given in Table VI. The comparatively small sample masses used in the present experiment lead to corrections of only $\sim 2\%$ except for the lowest neutron energies. In the work of Winters *et al.* [9], the samples were 3 to 4 times more massive, resulting in sizable corrections.

IV. RESULTS FOR THE NEUTRON CAPTURE CROSS SECTIONS

The neutron capture cross-section ratios of the samarium isotopes relative to ^{197}Au are listed together with the respective statistical, systematic, and total uncertainties in Table VII. The individual data for the three runs and the two evaluations discussed in Sec. III are given in Ref. [12]. Table VII contains the weighted average of the three runs, the weight being determined as the reciprocal of the square of the statistical uncertainties. No systematic differences were found in the data as obtained from different evaluations or different runs. This is particularly important for the comparison of runs II and III, which were made with different data acquisition modes.

As in our first experiments [2,6], the results of evaluation 2 were adopted as the final cross section ratios. The chosen energy binning is fine enough to avoid systematic uncertainties in the calculation of the Maxwellian-averaged cross sections (see Sec. VI). The final uncertainty in the cross-section ratio is of the order of 1%. This is a significant improvement compared with other experimental techniques.

The experimental ratios were converted into absolute cross sections by means of the gold cross section of Macklin [27], after normalization by a factor of 0.989 to the absolute value of Ratynski and Käppeler [28]. These

results are given in Table VIII. If these data are used in further work, their uncertainties can be calculated from the uncertainty of the cross-section ratio by adding quadratically the 1.5% uncertainty of the gold standard.

If we compare our results with the data from the literature, we find the following: The present results are significantly lower than those of the older experiments by Mizumoto for ^{147}Sm and ^{149}Sm [29] and by Shaw *et al.* for ^{149}Sm [30]. In the experiments by Kononov *et al.* [31,32], all isotopes covered in the present experiment were investigated, and the same behavior is observed, the discrepancies being up to factors of 2. This cannot be explained by the systematic uncertainties inherent in the different experimental methods, but is probably due to absorption of water in the samples as discussed in Ref. [10]. In more recent experiments, this problem was avoided and consequently better agreement is found. If we normalize the data of Winters *et al.* [9] in the same way as the present results, excellent agreement is found for ^{148}Sm and ^{150}Sm in the energy range from 15 to 200 keV. However, for ^{149}Sm the present data are higher by $\sim$20% in this range. This discrepancy might be explained by the fact that, as discussed already, ^{149}Sm is an isotope with very high multiplicity capture cascades. Consequently, it exhibits a very soft capture gamma-ray spectrum, while it is known that the spectrum of gold is hard by comparison. Thus, recently discovered problems with the weighting function [33] led to a systematic underestimate of the cross section in a relative measurement. It is hard to believe that this effect can cause a difference of 20%, but one has to keep in mind that discrepancies of this size have also been observed, in the opposite direction, for the 1.15 keV resonance in iron, where the capture gamma-ray spectrum is known to be extremely hard [34,35]. In the energy range below 15 keV, severe discrepancies were found for all three isotopes with maximum values up to 30% at 3 keV. This is due to systematic uncertainties in the subtraction of the scattering background, a highly uncertain procedure in experiments without resolution in gamma-ray energy. Good agreement is found with the recent experiment on ^{147}Sm and ^{152}Sm by Bochovko *et al.* [36], but slight differences in the cross-section shape are observed; their data tend to be lower than the present results at high energy. The unpublished data of Macklin [37] for ^{147}Sm and ^{149}Sm are lower by 7 and 10%, respectively, but the shape of the cross-section curve is in agreement down to 3 keV neutron energy. A recent experiment on ^{147}Sm by Gerstenhöfer [38], using Moxon-Rae detectors, is within the quoted uncertainty of 6%, in good agreement with the present data. In summary, it has to be emphasized that the uncertainties of the present data are significantly lower than for all previous experiments.

V. DISCUSSION OF UNCERTAINTIES

The determination of the statistical and systematic uncertainties of the present experimental method has been described in Refs. [2,6]. In the following, we briefly consider only new aspects inherent in the present experiment on the samarium isotopes. The individual uncertainties are compiled in Table IX.

(i) *Background subtraction.* In contrast to the tellurium experiment [6], the large cross sections of the samarium isotopes led to a favorable signal to background ratio. Thus the data could be evaluated down to 3 keV neutron energy. Assuming a systematic uncertainty of even 1% for the scattering subtraction correction, which is rather

TABLE VI. Correction factor $F_2 = \mathrm{MS(Au)}/\mathrm{MS}(X)$ for the cross-section ratio. Two values are given for each ratio corresponding to the gold samples Au I or Au II used in run 1 and runs 2,3, respectively.

Energy range (keV)	Correction for cross-section ratio, F_2				
	^{147}Sm/Au	^{148}Sm/Au	^{149}Sm/Au	^{150}Sm/Au	^{152}Sm/Au
3–5	0.959 0.955	1.110 1.104	0.960 0.955	1.116 1.111	1.100 1.094
5–7.5	0.966 0.972	1.069 1.075	0.972 0.978	1.058 1.064	1.046 1.052
7.5–10	0.978 0.984	1.053 1.059	0.983 0.988	1.033 1.039	1.026 1.032
10–12.5	0.984 0.990	1.045 1.052	0.987 0.994	1.022 1.029	1.017 1.024
12.5–15	0.986 0.995	1.038 1.047	0.988 0.997	1.021 1.030	1.012 1.021
15–20	0.988 0.997	1.028 1.037	0.988 0.997	1.009 1.018	1.005 1.014
20–25	0.991 1.000	1.020 1.029	0.988 0.997	1.004 1.013	1.001 1.010
25–30	0.992 1.002	1.014 1.024	0.988 0.998	1.001 1.011	0.998 1.008
30–40	0.993 1.003	1.007 1.017	0.986 0.996	0.997 1.007	0.995 1.005
40–50	0.994 1.004	1.001 1.011	0.985 0.995	0.996 1.006	0.994 1.004
50–60	0.996 1.006	0.998 1.008	0.985 0.995	0.996 1.006	0.993 1.003
60–80	0.997 1.006	0.996 1.005	0.986 0.995	0.997 1.006	0.993 1.002
80–100	0.999 1.008	0.994 1.003	0.987 0.996	0.997 1.006	0.993 1.002
100–120	0.999 1.008	0.993 1.002	0.987 0.996	0.995 1.004	0.993 1.002
120–150	0.999 1.007	0.993 1.001	0.988 0.996	0.994 1.002	0.993 1.001
150–175	1.000 1.007	0.994 1.001	0.989 0.996	0.994 1.001	0.994 1.001
175–200	1.000 1.006	0.994 1.000	0.989 0.995	0.993 0.999	0.993 0.999
200–225	1.000 1.005	0.995 1.000	0.989 0.994	0.994 0.999	0.994 0.999
Accuracy (%)	0.2	0.2	0.2	0.2	0.2

conservative, produces a systematic uncertainty in the low energy bins that is still small compared with the statistical uncertainty. Therefore, this uncertainty was neglected. This is confirmed by the fact that very good agreement is found in the shape of the cross-section curve with the data of Bochovko *et al.* [36] and Macklin [37].

On the other hand, the experiment of Winters *et al.* [6], where the same neutron source was used, shows significant deviations in the cross-section shape at low energies. Since C_6D_6 detectors were used in that experiment, which do not yield information on gamma-ray energy, it was not possible to determine the normalization of the spectrum measured with the carbon sample as a function of the neutron energy. As shown in Ref. [12] these corrections, indeed, depend on energy, and are different in shape for the samarium isotopes and the gold standard. Therefore, the assumption of a constant normalization factor made in the work of Ref. [6] would have led to systematic uncertainties at low energies, where the signal to background ratio is small.

(ii) *Flight path.* The flight path was measured several times during the experiment and was found to be reproducible within ±0.1 mm. Although the sample thickness varied between 0.3 and 2.6 mm, the mean flight path of the samples agreed within ±0.2 mm. Therefore, the uncertainty of 0.1% quoted in Ref. [2] was found to be a reasonable estimate for the present experiment also.

(iii) *Sample mass.* The careful analyses of the sample

TABLE VII. The final neutron capture cross section ratios of ^{147}Sm, ^{148}Sm, ^{149}Sm, ^{150}Sm, and ^{152}Sm relative to ^{197}Au together with the statistical and systematic uncertainties in (%).[a]

Energy (keV)	$\frac{\sigma(^{147}\text{Sm})}{\sigma(^{197}\text{Au})}$	Uncertainty stat	sys	tot	$\frac{\sigma(^{148}\text{Sm})}{\sigma(^{197}\text{Au})}$	Uncertainty stat	sys	tot	$\frac{\sigma(^{149}\text{Sm})}{\sigma(^{197}\text{Au})}$	Uncertainty stat	sys	tot
3–5	1.473	8.6	0.7	8.6	0.3198	9.8	0.7	9.8	3.331	6.0	0.7	6.0
5–7.5	1.423	4.5	0.7	4.5	0.3358	4.7	0.7	4.7	3.232	3.0	0.7	3.1
7.5–10	1.807	3.0	0.7	3.1	0.3391	3.5	0.7	3.5	3.564	2.1	0.7	2.2
10–12.5	1.577	2.3	0.7	2.4	0.3255	2.6	0.7	2.7	3.376	1.6	0.7	1.7
12.5–15	1.844	2.0	0.7	2.1	0.3710	2.1	0.7	2.2	3.632	1.4	0.7	1.6
15–20	1.730	1.2	0.7	1.4	0.3744	1.3	0.7	1.5	3.516	0.9	0.7	1.1
20–25	1.864	1.0	0.7	1.2	0.4305	1.0	0.7	1.2	3.604	0.7	0.7	1.0
25–30	1.732	0.9	0.7	1.1	0.3897	0.9	0.7	1.1	3.176	0.6	0.7	0.9
30–40	1.680	0.7	0.7	1.0	0.4148	0.6	0.7	0.9	3.003	0.5	0.7	0.9
40–50	1.691	0.7	0.7	1.0	0.4488	0.6	0.7	0.9	2.990	0.5	0.7	0.9
50–60	1.712	0.7	0.7	1.0	0.4523	0.6	0.7	0.9	2.912	0.5	0.7	0.9
60–80	1.682	0.6	0.7	0.9	0.4651	0.5	0.7	0.9	2.841	0.4	0.7	0.8
80–100	1.679	0.6	0.7	0.9	0.5155	0.5	0.7	0.9	2.859	0.4	0.7	0.8
100–120	1.643	0.6	0.7	0.9	0.5218	0.5	0.7	0.9	2.776	0.4	0.7	0.8
120–150	1.553	0.6	0.7	0.9	0.5367	0.5	0.7	0.9	2.743	0.4	0.7	0.8
150–175	1.499	0.7	0.7	1.0	0.5470	0.6	0.7	0.9	2.744	0.5	0.7	0.9
175–200	1.444	0.8	0.7	1.1	0.5612	0.6	0.7	0.9	2.754	0.5	0.7	0.9
200–225	1.438	1.2	0.7	1.4	0.5693	1.0	0.7	1.2	2.771	0.8	0.7	1.1

Energy	$\frac{\sigma(^{150}\text{Sm})}{\sigma(^{197}\text{Au})}$	Uncertainty	$\frac{\sigma(^{152}\text{Sm})}{\sigma(^{197}\text{Au})}$	Uncertainty
3–5	0.5354	9.5 0.7 9.5	0.6398	7.4 0.7 7.4
5–7.5	0.5561	4.5 0.7 4.5	0.5795	3.8 0.7 3.9
7.5–10	0.6077	3.0 0.7 3.1	0.6883	2.6 0.7 2.7
10–12.5	0.5912	2.2 0.7 2.3	0.6709	1.9 0.7 2.0
12.5–15	0.6781	1.9 0.7 2.0	0.7174	1.7 0.7 1.8
15–20	0.6666	1.1 0.7 1.3	0.7659	1.0 0.7 1.2
20–25	0.7698	0.9 0.7 1.1	0.8777	0.8 0.7 1.1
25–30	0.6608	0.8 0.7 1.1	0.8310	0.7 0.7 1.0
30–40	0.7087	0.6 0.7 0.9	0.8637	0.5 0.7 0.9
40–50	0.7779	0.6 0.7 0.9	0.8678	0.5 0.7 0.9
50–60	0.7837	0.5 0.7 0.9	0.9180	0.5 0.7 0.9
60–80	0.8131	0.4 0.7 0.8	0.9063	0.5 0.7 0.9
80–100	0.8943	0.4 0.7 0.8	0.9655	0.5 0.7 0.9
100–120	0.9044	0.5 0.7 0.9	0.9648	0.5 0.7 0.9
120–150	0.9620	0.5 0.7 0.9	0.7982	0.5 0.7 0.9
150–175	0.9803	0.5 0.7 0.9	0.6769	0.6 0.7 0.9
175–200	1.0095	0.6 0.7 0.9	0.6293	0.7 0.7 1.0
200–225	1.0273	0.9 0.7 1.1	0.5967	1.0 0.7 1.2

[a]Energy bins as used for the calculation of the Maxwellian-averaged cross sections.

TABLE VIII. The neutron capture cross section of ^{147}Sm, ^{148}Sm, ^{149}Sm, ^{150}Sm, and ^{152}Sm calculated from the experimental ratios using the gold data from literature [26,27].

Energy (keV)	$\sigma(^{197}\text{Au})$ (mb)	$\sigma(^{147}\text{Sm})$ (mb)	$\sigma(^{148}\text{Sm})$ (mb)	$\sigma(^{149}\text{Sm})$ (mb)	$\sigma(^{150}\text{Sm})$ (mb)	$\sigma(^{152}\text{Sm})$ (mb)
3–5	2266.7	3339.9	724.9	7550.5	1213.6	1450.2
5–7.5	1726.7	2456.2	579.8	5581.1	960.2	1000.6
7.5–10	1215.7	2197.3	412.2	4332.8	738.8	836.8
10–12.5	1066.7	1682.3	347.2	3601.5	630.6	715.7
12.5–15	878.0	1619.0	325.8	3189.1	595.4	629.8
15–20	738.8	1278.3	276.6	2597.4	492.4	565.8
20–25	600.0	1118.6	258.3	2162.3	461.9	526.6
25–30	570.8	988.6	222.4	1812.7	377.2	474.4
30–40	500.4	840.8	207.6	1502.8	354.6	432.2
40–50	433.3	732.9	194.5	1295.6	337.1	376.0
50–60	389.6	667.2	176.2	1134.5	305.4	357.7
60–80	349.4	587.6	162.5	992.5	284.1	316.6
80–100	298.3	500.7	153.8	853.0	266.8	288.0
100–120	290.1	476.6	151.4	805.3	262.4	279.9
120–150	274.1	425.7	147.1	752.0	263.7	218.8
150–175	263.7	395.2	144.2	723.5	258.5	178.5
175–200	252.6	364.7	141.8	695.6	255.0	159.0
200–225	248.5	357.2	141.4	688.5	255.3	148.3

material showed that water contamination could be excluded as their weight was determined with an uncertainty of 0.17%. Also, no deviations from the assumed stoichiometry could be observed in these analyses. Chemical impurities, mostly due to the rare earth elements neodymium and praseodymium, were determined to be less than 0.2%. Since these isotopes have comparable capture cross sections, a corresponding uncertainty of 0.2% was assumed for the sample mass.

(iv) *Isotopic enrichment.* In the present experiment, the enrichment of the main isotope was between 95 and 99 %, and the isotopic composition quoted by the suppliers was well confirmed by the measurements at KfK. Hence, a systematic uncertainty of 0.1% is assumed for the abundance of the main isotope. The uncertainties for the isotopic admixtures are negligible, even for the largest corrections in the case of the ^{148}Sm sample.

(v) *Isotopic correction.* The uncertainty discussed above refers to the number of atoms in the sample $m(X)$ [see Eq.(1)]. An additional uncertainty comes from the fact that part of the count rate Z_i is removed to account for the other isotopes as described in Sec. III B. In the present experiment, this correction is significant for the even isotopes with a maximum of 8% at ^{148}Sm (see Fig. 3). In that case, the 3.6% isotopic contribution of ^{147}Sm and ^{149}Sm carry an uncertainty of 2%, which results in an uncertainty of 0.2% for the cross section of the ^{148}Sm isotopes. For all other samples, this uncertainty was always less than 0.1%.

TABLE IX. Systematic uncertainties (%).

Flight path (cross-section ratio)		0.1
Neutron flux normalization (cross-section ratio)		0.2
Sample mass (samarium isotopes)		0.2
Isotopic enrichment (samarium isotopes)		0.1
Isotopic correction (^{148}Sm sample)		0.2
Isotopic correction (other Sm samples)		0.1
Multiple scattering (cross-section ratio)		0.2
Unobserved events (cross-section ratio Sm/Au)		0.6
	(ratio ^{148}Sm/^{150}Sm)	0.4
Total	σ(Sm)/σ(Au)	0.7
Systematic uncertainties	$\sigma(^{148}\text{Sm})/\sigma(^{150}\text{Sm})$	0.6

(vi) *Dead-time and pile-up.* Systematic uncertainties correlated with these effects were discussed in Ref. [2], and were found to be negligible.

(vii) *Normalization to equal neutron flux.* The corresponding normalization factors to equal neutron flux are similar to those of the tellurium experiment [6]; therefore, we assume the same systematic uncertainty of 0.2% for the cross section ratio.

(viii) *Spectrum fraction.* The systematic uncertainty due to the fraction of unobserved capture events, F_1 [see Eq. (1)], was discussed in detail in Ref. [2], where a systematic uncertainty of 0.6% was found. That discussion is also valid for the present experiment, but with a few improvements. In the present work, all cascades up to multiplicity 7 were included in the calculations, even for the gold sample. Also, the variation of the energy threshold between 0 and 100 keV is irrelevant for capture in the odd samarium isotopes since no transitions below 100 keV are observed in the compound nucleus. Therefore, the previously quoted uncertainty of 0.6% can also be adopted for the cross-section ratios of the samarium isotopes and the gold standard. For the final application of the data in *s*-process studies (see Sec. VII), where only the cross-section ratio $\sigma(^{148}\text{Sm})/\sigma(^{150}\text{Sm})$ is important, this uncertainty is even smaller because the uncertainty in the gold cross section cancels out.

(ix) *Multiple scattering and self-shielding.* The comparatively large cross sections of the samarium isotopes

allowed the use of small samples. Consequently, the multiple scattering and self-shielding correction, F_2 (see Table VI), is less than $\sim 1\%$ for most of the energy range and for all cross-section ratios. This is about two to five times smaller than the F_2 values for the tellurium isotopes [6]. Since the total cross sections were determined simultaneously in this experiment with an accuracy of 5–10 %, the correlated uncertainties should be reduced by a factor of 2.

These estimates of the systematic uncertainties are correct for most of the energy range, but seem somewhat optimistic below ~ 10 keV neutron energy. In this range, however, the statistical uncertainties are increasing rapidly and dominate the total uncertainty. Thus, an energy-dependent systematic uncertainty for the multiple scattering correction would have no influence on the final results.

(x) *Absorption of water in the samples.* As discussed in Sec. III, the water absorbed at their surface corresponded to 0.2% of the sample mass. The plastic cladding yielded an additional water equivalent of $\sim 0.2\%$, but affected the gold reference, too. The respective systematic uncertainties for the samples are difficult to estimate, since we do not have an appropriate computer code to include the moderation effect of this hydrogen contamination. The only quantitative hints come from the work of Mizumoto and Sugimoto [10], who calculated a correction of 17% at 100 keV neutron energy for a 5.2% water contamination of a sample that was 2.3 times thicker and 36 times heavier than those of this experiment. According to this comparison and since the effect of the plastic foil cancels out to some extent in the relative measurement, we are sure that the small hydrogen impurity has no noticeable effect on our results.

VI. MAXWELLIAN-AVERAGED CROSS SECTIONS

The Maxwellian-averaged cross sections were calculated in the same way as described in Refs. [2] and [39]. The neutron energy range from 0 to 700 keV was divided into three parts according to the cross sections from different sources. The respective contributions I_x are tabulated in Ref. [12]. The values I_2 covering the neutron energy range from 3 to 225 keV were calculated using the cross sections of the present experiment given in Table VIII. The chosen energy bins are fine enough to neglect the correlated systematic uncertainties that may result from a coarse energy grid.

The contributions I_1 from the energy range 0 to 3 keV were determined in two different ways. Statistical model calculations were performed and the parameters were adjusted so that the calculated cross sections fitted the data of the present experiment at energies above 3 keV and the data that were calculated from resonance parameters [26] at low energies. In the second calculation we used the cross sections of the joint evaluated file [17] which were averaged in the energy range from 0 to 10 keV in 0.5 keV wide bins. These data were normalized to the present experiment in the overlap region from 3 to 10 keV. Though the respective normalization factors were ranging from 0.864 to 1.229, the energy dependence of both data sets was found in good agreement except for ^{147}Sm. That results from the second calculation were systematically higher may be due to the fact that the cross sections calculated from resonance parameters underestimate the true cross section because of missing resonances. The final data are the averages of the two calculations, which agreed in general within the adopted uncertainty of 10%.

The energy interval from 225 to 700 keV, which contributes only very little to the Maxwellian average at typical *s*-process temperatures, was covered by again normalizing the JEF data to the present experiment in the energy interval from 100 to 200 keV. The uncertainties were calculated under the assumption that the uncertainty of the normalized cross sections increases from 2% at 225 keV to 10% at 700 keV. The final results are given in Table X.

We note that, in determining ratios, e.g., $\langle\sigma\rangle(^{148}\mathrm{Sm})/\langle\sigma\rangle(^{150}\mathrm{Sm})$, it is not permissible to add the uncertainties given in Table X quadratically, because they are strongly correlated. For example, the statistical

TABLE X. Maxwellian-averaged neutron capture cross sections of the samarium isotopes 147 to 152. The uncertainty of 1.5% of the gold standard is not included in the quoted uncertainty since it cancels out in most applications of relevance for nuclear astrophysics (see Sec. VII).

kT (keV)	^{147}Sm (mb)	^{148}Sm (mb)	^{149}Sm (mb)	^{150}Sm (mb)	^{152}Sm (mb)
10	1962.9±43.4	414.9±8.7	4016.9±83.2	742.3±16.0	863.3±19.3
12	1736.2±32.8	373.6±6.5	3504.3±61.9	665.0±12.0	771.8±14.3
20	1246.3±15.9	286.6±3.3	2409.1±28.6	504.8±5.8	581.2±6.8
25	1085.4±12.1	259.3±2.5	2059.1±21.3	455.3±4.6	518.6±5.3
30	973.1±10.0	240.7±2.2	1819.9±17.2	421.9±3.8	473.2±4.4
40	824.3±7.7	217.2±1.8	1515.0±13.0	380.1±3.2	409.5±3.5
50	729.0±6.5	203.2±1.6	1328.9±10.8	354.6±2.9	364.6±3.0
52	713.7±6.3	201.1±1.6	1300.0±10.5	350.4±2.9	357.2±3.0
60	661.8±5.8	194.0±1.7	1202.8±9.8	336.6±2.7	330.9±2.7
70	611.6±5.5	187.6±1.7	1111.0±9.3	322.9±2.8	304.4±2.6
80	572.6±5.5	182.7±1.9	1040.2±9.5	311.6±3.0	282.8±2.5
90	540.8±5.7	178.8±2.2	983.1±10.0	301.9±3.3	265.1±2.6
100	514.4±6.1	175.2±2.4	935.4±10.8	293.3±3.7	250.0±2.7

uncertainties of the cross-section ratios are partly determined by the count rate in the gold spectra [Z_i(Au), $\sum Z$(Au), $\sum E$(Au) in Eq. 1] which cancels out in the cross-section ratio for two samarium isotopes. The same holds for the systematic uncertainties for multiple scattering and for the spectrum fraction of the gold sample. The proper uncertainty of the ratio of Maxwellian-averaged cross sections of two samarium isotopes was evaluated explicitly for the s-only isotopes ^{148}Sm and ^{150}Sm, and was found to be $\sim$30% lower than expected from a quadratic summation (Table XI).

If the present results at $kT=30$ keV are compared with the data given in the compilation of Bao and Käppeler [11], one finds the same discrepancies as discussed above. That our data for ^{148}Sm and ^{150}Sm are lower by 9% and 6% compared with the results of Winters *et al.* [9] is somewhat surprising in view of the good agreement in the energy range from 15 to 200 keV, indicating the significant contribution of the low energy region to the Maxwellian average. It should be noted, however, that the ratio, $\langle\sigma\rangle(^{148}\text{Sm})/\langle\sigma\rangle(^{150}\text{Sm})$, the quantity of astrophysical importance, is in agreement at $kT=30$ keV within the quoted uncertainties. In any case, the uncertainty of this ratio has been improved by a factor of 4 by the present results.

It is also interesting to see the good agreement with the pioneering work of Macklin and Gibbons [40], who were the first to measure these samarium cross sections about 30 years ago. Their results are given with uncertainties of 15 to 20%, but within these limits the data agree for all five measured isotopes with the present values. The result of Beer *et al.* [41] obtained in an activation experiment for ^{152}Sm is significantly lower than the present value.

VII. IMPLICATIONS FOR THE CLASSICAL s PROCESS AND FOR A STELLAR MODEL

With the accurate (n,γ) cross sections of the samarium isotopes of the present work, four aspects of s-process nucleosynthesis can be improved: The reaction flow in the s process is expressed by the smooth $\langle\sigma\rangle N_s(A)$ curve, and can be normalized to the corresponding empirical product for ^{150}Sm, since this isotope experiences the entire s-process flow. Together with a similar normalization point at ^{124}Te, which has been investigated in a previous study [6], it is now possible to define the steplike decrease of the $\langle\sigma\rangle N_s$ curve at the neutron magic nuclei with $N=82$—and hence the mean neutron exposure, τ_0—with better reliability. A second result concerns the information on neutron density, which can be inferred from the s-process branchings at $A=147$, 148, and 149. The strength of these branchings is reflected by the $\langle\sigma\rangle N_s$ ratio of ^{148}Sm and ^{150}Sm (see Fig. 1). Since the abundance ratio is practically given by the isotopic ratio of the two nuclei, the present cross sections allow an improved determination of the neutron density in the s process, which is the relevant parameter for these branchings. The present data can also be used for testing the neutron density and temperature profiles predicted by a stellar model for helium shell burning in low mass stars that originates from the work of Iben and Renzini [42], and Hollowell and Iben [43,44], and has been used successfully for nucleosynthesis studies by Gallino *et al.* [3,4,45]. Finally, the interpretation of recently discovered isotopic anomalies in meteoritic samarium [46] as genuine s-process material can be checked with the new cross sections.

TABLE XI. The ratio of the Maxwellian-averaged neutron capture cross sections of ^{148}Sm and ^{150}Sm and the correlated uncertainty.

kT (keV)	$\langle\sigma\rangle(^{148}\text{Sm})/\langle\sigma\rangle(^{150}\text{Sm})$
10	0.559±2.8%
12	0.562±2.3%
20	0.568±1.4%
25	0.570±1.1%
30	0.571±1.0%
40	0.571±0.8%
50	0.573±0.8%
52	0.574±0.8%
60	0.576±0.8%
70	0.581±0.9%
80	0.586±1.1%
90	0.592±1.4%
100	0.597±1.7%

A. Normalization of the $\langle\sigma\rangle N_s$ curve

The discussion in this and the next subsection refers to the classical approach for the s process. The general formalism and the respective terminology have been outlined in Ref. [5], and the particular problem of the Nd-Pm-Sm region was addressed in full detail in Ref. [9]. Therefore, the discussion will be restricted here to the most essential features.

For $A>90$, the mass flow along the s-process nucleosynthesis path between iron and bismuth is dominated by the so-called main component. The abundances produced by this main component were found to be the result of an exponential distribution of neutron exposures, $\rho(\tau)$, to which a fraction G of the observed iron abundance $N_\odot$ was exposed. By this approach and with some simplifying assumptions, the system of coupled differential equations describing the s-process flow can be solved analytically [7]. The resulting characteristic product of cross section times s abundance can be written as

$$\langle\sigma\rangle N_s(A)=\frac{GN_{\text{Fe},\odot}}{\tau_0}\prod_{i=56}^{A}\left[1+\frac{1}{\langle\sigma\rangle_i\tau_0}\right]^{-1}.$$

The free parameters, G and τ_0, are determined by a least squares fit to the empirical $\langle\sigma\rangle N_s$ values of those s-only nuclei that experience the entire s-process flow. Hence, these normalization points should not be affected by significant branchings in the synthesis path. Obviously, the quality of this fit depends on the uncertainties of the respective empirical $\langle\sigma\rangle N_s$ values. The relative contributions from the observed abundances vary from $<2\%$ for the lanthanides up to $\sim$10% for more volatile elements [47]. In practically all relevant cases, the respec-

tive cross-section uncertainties are between 5 and 10%. Since there are about 10 such normalization points for fitting only two parameters, the system is overdetermined and the problem of uncertainties is correspondingly reduced. The mean exposure was determined [3] to be

$$\tau_0=(0.306\pm0.010)\left[\frac{kT[\text{keV}]}{30}\right]^{1/2}\text{mb}^{-1}\ .$$

With the availability of cross sections that are accurate to $\pm1\%$, this fit to the normalization points of the $\langle\sigma\rangle N_s$ curve can be improved correspondingly. The first two nuclei in this category are ^{124}Te [6] and ^{150}Sm, one below and the other above the step in the $\langle\sigma\rangle N_s$ curve at magic neutron number $N=82$. Since this step is determined by the mean neutron exposure, these two isotopes would be sufficient to derive an improved value for τ_0, if the Te and Sm abundances were sufficiently accurate. The mean exposure that results directly from the $\langle\sigma\rangle N_s$ values of ^{124}Te and ^{150}Sm is

$$\tau_0=(0.303\pm0.010)\left[\frac{kT[\text{keV}]}{30}\right]^{1/2}\text{mb}^{-1}$$

in excellent agreement with the value of Ref. [3]. However, the uncertainty assigned to the Te abundance is 10% [47]. Therefore, the only conclusion to be drawn at this point is that the uncertainty of the Te abundance may have been overestimated in Ref. [47], and could be reduced to about 3%, based on the observed $\langle\sigma\rangle N_s$ systematics.

B. The *s*-process neutron density

As illustrated in Fig. 1, the *s*-process path in the Nd-Pm-Sm region exhibits branchings due to the competition between neutron captures and beta decays at ^{147}Nd and at the Pm isotopes. The combined strength of these branchings manifests itself in the difference of the $\langle\sigma\rangle N_s$ values of ^{148}Sm (which is partly bypassed) and ^{150}Sm (which experiences the entire *s*-process flow). The respective branching factors,

$$f_-=\frac{\lambda_\beta}{\lambda_\beta+\lambda_n}\ ,$$

can therefore be combined to an effective factor,

$$f_-^{\text{eff}}=\frac{\langle\sigma\rangle N_s(^{148}\text{Sm})}{\langle\sigma\rangle N_s(^{150}\text{Sm})}\ .$$

Since the beta decay rates, $\lambda_\beta=\ln2/t_{1/2}$, at the branching points in Fig. 1 are not significantly affected by temperature, the set of equations summarized in the above expressions (for an explicit discussion, see Ref. [9]) can be solved for the neutron capture rate $\lambda_n=\langle\sigma\rangle v_T n_n$ in order to obtain an estimate for the *s*-process neutron density, n_n.

Compared with the previous result of Winters *et al.* [9] ($f_-^{\text{eff}}=0.92\pm0.04$), the present measurement yields a considerably more precise value, $f_-^{\text{eff}}=0.870\pm0.009$, with a 4 times smaller uncertainty. Adopting all other quantities from Ref. [9], and considering complete thermal equilibrium in the population of isomer and ground state in ^{148}Pm [3,48], one arrives at a neutron density

$$n_n=(3.8\pm0.6)\times10^8\ \text{cm}^{-3}\ ,$$

in excellent agreement with the result of Ref. [3], where $(3.4\pm1.1)\times10^8$ cm^{-3} was reported. Because of the improved samarium cross sections, the uncertainty of n_n is no longer dominated by the uncertainty of f_-^{eff}, but by the uncertainties of the calculated cross sections for the unstable branch point isotopes. This problem will be addressed below.

At this level of accuracy, *p*-process corrections may no longer be negligible. Until recently, quantitative *p*-process models were missing. Therefore, *p*-process corrections were based on empirical estimates deduced from abundance trends of nearby *p*-only nuclei [49]. For ^{148}Sm and ^{150}Sm, this method yields corrections of 1.1 and 1.7%, respectively, leading to a marginal effect on the neutron density [$n_n=(3.6\pm0.6)\times10^8$ cm^{-3}]. The *p*-process corrections that result from recent model calculations ([50–52], and private communications by these authors) indicate smaller corrections of 0.7 and 0.3%, on average, for ^{148}Sm and ^{150}Sm, with a correspondingly smaller impact for the neutron density. In summary, the best estimated *p*-process corrections to the abundances of the *s*-only samarium isotopes imply no significant effect on the estimates of τ_0 or the neutron density.

A remaining uncertainty concerns the (n,γ) cross sections of the unstable promethium isotopes. Recently, the capture cross section of ^{147}Pm has been measured for the first time [38]. Despite experimental difficulties, an uncertainty of 15% could be claimed for this cross section. This new value, a factor of 2 smaller than predicted by the detailed model calculation of Ref. [9], leads to a neutron density, $n_n=4.1\times10^8$ cm^{-3}, similar to the solution based on the calculated ^{147}Pm cross section. However, this discrepancy between experiment and theory could be particularly serious if it reflects a general problem of the cross-section calculation in the vicinity of the closed neutron shell $N=82$. Scaling the calculated cross sections of the other promethium isotopes by the same factor of 2 would increase the neutron density to 5.4×10^8 cm^{-3}. Therefore, the ^{147}Pm cross section requires verification, both experimentally and repeating the statistical model calculations with an updated set of input parameters.

C. Comparison with a stellar model

The stellar model that has been shown to reproduce the *s*-process abundances quite well [3,4,42–45] refers to helium shell burning in low mass stars with about $\frac{1}{3}$ of the solar metallicity. In this scenario, relatively short helium burning episodes, where neutrinos are released in (α,n) reactions on ^{13}C and ^{22}Ne alternate with much longer periods when the consumed helium is replenished by hydrogen burning. An exponential distribution of neutron exposures is naturally achieved in this model by the fractional overlap of zones containing freshly synthesized material. (For a detailed discussion see the references quoted above.)

The profiles for the effective neutron density and tem-

perature during the helium burning episodes have been deduced from the more detailed model [53] and were used with the network code NETZ [54] to follow the *s*-process flow in the entire mass region from Fe to Bi. On average, the *s*-only isotopes are well reproduced for $A > 90$ in this calculation. However, with the accurate cross sections now available for the tellurium and samarium isotopes, significant discrepancies are emerging in the calculated abundance patterns of the respective branchings. In the present case, the model yields an overproduction of 6% for ^{148}Sm, corresponding to 6 standard deviations in terms of the cross-section uncertainty. Since this discrepancy is also not very sensitive to the above mentioned problem of the promethium cross sections, it may be a hint that the neutron density is underestimated by the model.

However, any increase of the neutron density would also increase the problem related to the abundances of the *s*-only isotopes of tellurium, where the model overestimates the effect of the branchings at $A = 121$ and 122 [6]. Of the two possible solutions suggested for the Te puzzle [6]—either to increase the temperature or to decrease the neutron density—the second possibility can now be excluded by the present results. This shows that the combined analysis of the branchings defined by the *s*-isotopes of Te and Sm points to model inconsistencies with respect to temperature *and* neutron density.

In view of these problems, detailed investigations of additional branchings are required, in particular of cases that are more sensitive to temperature. On the other hand, it will be important to pursue attempts to improve the models for helium shell burning in low mass stars [53] or to search for an alternative stellar *s*-process scenario [55].

D. Isotopic anomalies

Recently, Richter *et al.* [46] reported on improved measurements of isotopic anomalies found in SiC grains of the Murchison meteorite. In particular, their observed abundance patterns for samarium imply that these grains consist of pure *s*-process material. This idea is strongly supported by the agreement with the abundances calculated for the *s*-process in low mass stars [56], or even with the simple assumption of a "local equilibrium" in the classical *s* process, that is, $\langle \sigma \rangle N_s = \text{const}$ for the samarium isotopes. If the latter assumption is replaced by the proper treatment of the branchings at $A = 147$, 148, and 149, the classical approach yields even better agreement with the observed anomalies. The full treatment with the classical approach yields abundance ratios

$$^{147}\text{Sm}/^{148}\text{Sm}/^{149}\text{Sm}/^{150}\text{Sm}/^{152}\text{Sm} = 1.72\pm0.50/6.68\pm0.09/1.00/4.28\pm0.05/3.55\pm0.04 ,$$

while the measured anomaly is given as [46]

$$2.09\pm0.17/6.41\pm0.30/1.00/4.30/4.68\pm0.35 .$$

The only serious discrepancy between these ratios concerns ^{152}Sm, where the new cross section results in a smaller abundance. However, this difference could partly be due to the effect of the branching at ^{151}Sm which needs further consideration. We note here that the problem with the ^{147}Sm abundance found by Richter *et al.* [46] in connection with the *s* abundances tabulated in Ref. [5] resulted from a missing line in that table which should have taken account of the decay of unstable ^{147}Pm. With this correction, Ref. [5] also confirms the present finding of the samarium anomalies being of *s*-process origin.

VIII. CONCLUSIONS

This second application of the Karlsruhe 4π BaF_2 detector confirmed that differential neutron capture cross sections in the range of astrophysical interest can be determined with an accuracy of $\pm 1\%$. It was the intention of the present work to discuss the difficulties and possible pitfalls thoroughly, and to present in detail the approaches and solutions in order to justify the claimed accuracy.

The (n,γ) cross sections were measured for a sequence of samarium isotopes, that define the *s*-process branchings at $A = 147$, 148, and 149. The experiment was carried out on ^{147}Sm, ^{148}Sm, ^{149}Sm, ^{150}Sm, and ^{152}Sm and covered the energy range from 3 to 225 keV. It was performed in different runs with modified experimental parameters. The good agreement in the respective regions of overlap is an important confirmation for the validity of the evaluation of corrections and systematic uncertainties. A novelty in the present measurement was the implementation of an ADC system for analyzing energy and time-of-flight information for each individual detector module. In this way, background corrections were improved and additional information was obtained on the energy spectrum and multiplicity of the capture gamma-ray cascades.

As in the previous experiment on the tellurium isotopes [6], a considerable effort was made to obtain a reliable characterization of the samples. Careful preparation and repeated analyses were found to be important in order to eliminate water contamination and to define sample mass and stoichiometry. Otherwise, significant effects could not have been excluded. Very likely, part of the discrepancies between the present data and previous results could result from this type of problem. However, the high gamma-ray multiplicity observed for the odd samarium isotopes could be another cause for discrepancies. Since the very soft gamma-ray spectrum of these isotopes differs significantly from the much harder spectrum of the gold reference sample, measurements using the pulse height weighting technique could well have been sensitive to this effect.

The Maxwellian-averaged cross sections that were calculated from the differential data are important for

several aspects of *s*-process nucleosynthesis. First, ^{150}Sm represents one of the major normalization points for the definition of the $\langle\sigma\rangle N_s$ curve, and hence of the *s*-process abundance distribution. Secondly, the strength of the *s*-process branchings at $A=147$, 148, and 149 can be quantified by comparison of the $\langle\sigma\rangle N$ values of the *s*-only pair ^{148}Sm and ^{150}Sm. The accurate determination of the cross-section ratio for these two nuclei removed the main uncertainty in the *s*-process neutron density, resulting in a significantly improved estimate, $n_n=(3.8\pm0.6)\times10^8$ cm^{-3}, via the classical approach. In addition, this ratio can also be considered as a sensitive test for the neutron density profile provided by stellar *s*-process models. Finally, the new cross sections allow for the better classification of isotopic anomalies in meteorites.

The remaining open problems are mostly due to the discrepancy between the recently measured (n,γ) cross section of the unstable branch point nucleus ^{147}Pm and the theoretical value based on a detailed statistical model calculation. Certainly, this problem requires more work, but improving the models for stellar *s*-process scenarios also requires more work in order to satisfy the constraint imposed by the *s*-process branching defined by the ^{148}Sm/^{150}Sm pair.

ACKNOWLEDGMENTS

The present work profited from the help of many colleagues from KfK. In particular we would like to thank Ch. Adelhelm, G. Streib, and M. Mackert from the Institute of Material Research for their careful analyses of the water and samarium content of the samples. We also appreciate the spontaneous help of E. Gantner, H. Deutsch, and H. Klewe-Nebenius, from the Institute of Radiochemistry, who determined the isotopic composition. We wish to thank F. H. Fröhner and B. Krieg, from the Institute of Neutron Research, who provided us with the data from the JEF evaluation. We gratefully acknowledge the analyses by *K* x-ray absorptiometry by H. Ottmar and H. Eberle, as well as the calculations with the transputer system by J. Oehlschläger. The Van de Graaff crew, D. Roller, E.-P. Knaetsch, and W. Seith, did a great job in keeping the accelerator running at optimum performance. Last but not least, we thank G. Rupp for his continuous support in optimizing the experimental setup.

[1] K. Wisshak, K. Guber, F. Käppeler, J. Krisch, H. Müller, G. Rupp, and F. Voss, Nucl. Instrum. Methods **A292**, 595 (1990).
[2] K. Wisshak, F. Voss, F. Käppeler, and G. Reffo, Phys. Rev. C **42**, 1731 (1990); Kernforschungszentrum Karlsruhe Report KfK-4674, 1990.
[3] F. Käppeler, R. Gallino, M. Busso, G. Picchio, and C. M. Raiteri, Astrophys. J. **354**, 630 (1990).
[4] R. Gallino, M. Busso, G. Picchio, C. M. Raiteri, and A. Renzini, Astrophys. J. **334**, L45 (1988).
[5] F. Käppeler, H. Beer, and K. Wisshak, Rep. Prog. Phys. **52**, 945 (1989).
[6] K. Wisshak, F. Voss, F. Käppeler, and G. Reffo, Phys. Rev. C **45**, 2470 (1992); Kernforschungszentrum Karlsruhe Report KfK-4899, 1991.
[7] D. D. Clayton, W. A. Fowler, T. E. Hull, and B. A. Zimmerman, Ann. Phys. **12**, 331 (1961).
[8] N. E. Holden, R. L. Martin, and I. L. Barnes, Pure Appl. Chem. **56**, 675 (1984); IUPAC International Union of Pure and Applied Chemistry, *ibid.* **63**, 991 (1991).
[9] R. R. Winters, F. Käppeler, K. Wisshak, A. Mengoni, and G. Reffo, Astrophys. J. **300**, 41 (1986).
[10] M. Mizumoto and M. Sugimoto, Nucl. Instrum. Methods **A282**, 324 (1989).
[11] Z. Y. Bao and F. Käppeler, At. Data Nucl. Data Tables **36**, 411 (1987).
[12] K. Wisshak, K. Guber, F. Voss, F. Käppeler, and G. Reffo, Kernforschungszentrum Karlsruhe Report KfK-5067, 1992.
[13] K. Guber, thesis, University of Karlsruhe, 1993 (unpublished).
[14] G. Winkler, Nucl. Instrum. Methods **A282**, 317 (1989).
[15] H. Ottmar, H. Eberle, L. Koch, R. de Meester, and E. Kuhn, *Proceedings of the International Symposium on Nuclear Material Safeguards,* Vienna, 1986 (International Atomic Energy Agency, Vienna, 1987); p. 201.
[16] R. de Meester, H. Eberle, S. Johnson, L. Koch, I. Michel-Piper, H. Nackaerts, and H. Ottmar, in [15], p. 233.
[17] C. Nordborg, H. Gruppelaar, and M. Salvatores, in *Proceedings of the International Conference on Nuclear Data for Science and Technology,* Jülich, Germany, 1991, edited by S. M. Qaim (Springer, Berlin, 1992), p. 782.
[18] V. McLane, C. L. Dunford, and P. F. Rose, *Neutron Cross Sections* (Academic, New York, 1988), Vol. 2.
[19] K. K. Seth, Phys. Lett. **16**, 306 (1965).
[20] G. Reffo, F. Fabbri, K. Wisshak, and F. Käppeler, Nucl. Sci. Eng. **80**, 630 (1982).
[21] K. Wisshak, F. Käppeler, and G. Schatz, Nucl. Instrum. Methods **221**, 385 (1984).
[22] H. J. Gils, D. Heck, J. Oehlschläger, G. Schatz, T. Thouw, and A. Merkel, Comput. Phys. Commun. **56**, 105 (1989).
[23] N. Weber, thesis, University of Karlsruhe, 1993 (unpublished).
[24] F. H. Fröhner, "SESH—A Fortran IV Code for Calculating the Self-Shielding and Multiple Scattering Effects for Neutron Cross-Section Data Interpretation in the Unresolved Resonance Region," Gulf General Atomic, Report GA-8380, 1968.
[25] A. Gilbert and A. G. W. Cameron, Can. J. Phys. **43**, 1446 (1965).
[26] S. F. Mughabghab, M. Divadeenam, and N. E. Holden, *Neutron Cross Sections* (Academic, New York, 1981), Vol. 1, Part A.
[27] R. L. Macklin, private communication.
[28] W. Ratynski and F. Käppeler, Phys. Rev. C **37**, 595 (1988).
[29] M. Mizumoto, Nucl. Phys. **A357**, 90 (1981).
[30] R. A. Shaw, W. R. Koste, and R. W. Hockenbury, unpublished.
[31] V. N. Kononov, B. D. Yurlov, G. E. Manturov, E. D.

Poletaev, and V. M. Timokhov, Yad. Fiz. **26**, 947 (1977) [Sov. J. Nucl. Phys. **26**, 500 (1977)].
[32] V. N. Kononov, B. D. Yurlov, E. D. Poletaev, and V. M. Timokhov, Yad. Fiz. **27**, 10 (1978) [Sov. J. Nucl. Phys. **27**, 5 (1978)].
[33] F. Corvi, A. Prevignano, H. Liskien, and P. B. Smith, Nucl. Instrum. Methods **A265**, 475 (1988).
[34] R. L. Macklin, Nucl. Sci. Eng. **83**, 309 (1983).
[35] R. L. Macklin, Nucl. Sci. Eng. **95**, 200 (1987).
[36] M. W. Bochovko, A. A. Woewodskij, V. N. Kononov, T. N. Manturov, E. D. Poletaev, and V. M. Timokhov, Fiziko Energetscheskij Institut, Obninsk, Report FEI-2168, 1991.
[37] R. L. Macklin, Reports EXFOR 12966.003 and .004, 1986.
[38] T. W. Gerstenhöfer, thesis, University of Heidelberg, 1993, unpublished.
[39] H. Beer, F. Voss, and R. R. Winters, Astrophys. J. Suppl. **80**, 403 (1992).
[40] R. L. Macklin and J. H. Gibbons, Astrophys. J. **149**, 577 (1967).
[41] H. Beer, F. Käppeler, K. Yokoi, and K. Takahashi, Astrophys. J. **278**, 388 (1984).
[42] I. Iben, Jr. and A. Renzini, Astrophys. J **259**, L79 (1982); **263**, L23 (1982).
[43] D. E. Hollowell and I. Iben, Jr., Astrophys. J. **333**, L25 (1988).
[44] D. E. Hollowell and I. Iben, Jr., Astrophys. J. **340**, 966 (1989).
[45] R. Gallino, M. Busso, and C. M. Raiteri, in *Nuclei in the Cosmos '92*, edited by F. Käppeler and K. Wisshak (Institute of Physics, Bristol, 1993), p. 509.
[46] S. Richter, U. Ott, and F. Begemann, in [46], p. 127.
[47] E. Anders and N. Grevesse, Geochim. Cosmochim. Acta **53**, 197 (1989).
[48] K. Lesko, E. B. Norman, R. M. Larimer, J. C. Bacelar, and E. M. Beck, Phys. Rev. C **39**, 619 (1989).
[49] H. Beer, Kernforschungszentrum Karlsruhe internal report, 1985 (unpublished).
[50] M. Rayet, N. Prantzos, and M. Arnould, Astr. Astrophys. **227**, 271 (1990).
[51] N. Prantzos, M. Hashimoto, M. Rayet, and M. Arnould, Astr. Astrophys. **238**, 455 (1990).
[52] W. M. Howard, B. S. Meyer, and S. E. Woosley, Astrophys. J. **373**, L5 (1991).
[53] R. Gallino, private communication.
[54] S. Jaag, thesis, University of Karlsruhe, 1990 (unpublished).
[55] I.-J. Sackmann, private communication.
[56] R. Gallino, C. M. Raiteri, and M. Busso, Astrophys. J. (submitted).